




Accumulation and depletion of *E. coli* in surfaces mediated by curvature

Benjamín Pérez-Estay ^{1,2,*}, María Luisa Cordero ¹, Néstor Sepúlveda ³, and Rodrigo Soto ¹

¹*Departamento de Física, FCFM, Universidad de Chile, Av. Beauchef 850, 8370458 Santiago, Chile*

²*Laboratoire PMMH-ESPCI Paris, PSL Research University, Sorbonne University, University Paris-Diderot, 7, Quai Saint-Bernard, 75005 Paris, France*

³*School of Engineering and Sciences, Universidad Adolfo Ibáñez, Diagonal las Torres 2640, Peñalolén, 7941169 Santiago, Chile*



(Received 7 August 2023; accepted 27 March 2024; published 1 May 2024)

Can topography be used to control bacteria accumulation? We address this question in the model system of smooth-swimming and run-and-tumble *Escherichia coli* swimming near a sinusoidal surface, and show that the accumulation of bacteria is determined by the characteristic curvature of the surface. For low curvatures, cells swim along the surface due to steric alignment and are ejected from the surface when they reach the peak of the sinusoid. Increasing curvature enhances this effect and reduces the density of bacteria in the curved surface. However, for curvatures larger than $\kappa^* \approx 0.25 \mu\text{m}^{-1}$, bacteria become trapped in the valleys, where they can remain for long periods of time. Minimal simulations considering only steric interactions with the surface reproduce these results and give insights into the physical mechanisms defining the critical curvature, which is found to scale with the inverse of the bacterial length. We show that for curvatures larger than κ^* , the otherwise stable alignment with the wall becomes unstable while the stable orientation is now perpendicular to the wall, thus predicting accurately the onset of trapping at the valleys.

DOI: [10.1103/PhysRevE.109.054601](https://doi.org/10.1103/PhysRevE.109.054601)

I. INTRODUCTION

Accumulation of bacteria at surfaces is the cause of many medical and industrial concerns. Examples are infections in medical implants [1–4], contamination of medical devices such as indwelling catheters [5], reduction of heat, mass, and liquid transfer due to pipe biofouling [6,7], and microplastic colonization in marine debris [8]. Bacteria roaming their environment are attracted to surfaces due to hydrodynamic effects or chemical signals [9,10], and when in contact with a surface, their adhesion is mediated by Lifshitz–van der Waals and electrostatic interactions [11,12]. Once adhered to the surface, the irreversible process of biofilm formation can begin, in which case bacteria secrete different proteins and polysaccharides that form an extracellular matrix shared by the cells. In biofilms, bacteria are able to resist antibiotics, the host immune system, and other hostile environments, making it a serious health issue [13–16]. Thus, it is desirable to prevent bacteria adhesion while the process is still reversible.

Traditional strategies to avoid bacterial adhesion to surfaces include chemical coatings, exposition to UV light, ultrasonic vibrations, and autoclaving [17,18]. However, not all methods yield long-lasting results or can be used in any surface. Control of surface topography has risen as a practical option, as its working principle is chemical free and can be used in implants. Some topographical designs to reduce bacteria accumulation include microscopic wells of nanometric depth homogeneously distributed in space [19], diamondlike patterns inspired in sharkskin [20], and hierarchically wrin-

kled surface topographies inspired by rose petal structures [21,22]. Typically, these patterns make the surface superhydrophobic or hydrophilic, which reduces adhesion [23]. Alternatively, these patterns can interrupt colony expansion by trapping the bacteria [24,25].

Another topographical approach consists of the control of surface curvature at a larger scale of tens of micrometers. Such surfaces can be easily incorporated in medical devices exposed to blood flow or in marine vessels. The working principle lies in breaking the hydrodynamic and steric interactions that exist between swimming bacteria and solid boundaries. Steric interactions act on bacteria as they approach a wall, producing a torque that causes them to align almost parallel to the surface, with a small angle towards the wall [26]. Once swimming parallel to the wall, hydrodynamic interactions maintain the cells near the wall and produce a torque that generates circular bacterial trajectories on the surface [27]. This leads to the hydrodynamic trapping of bacteria on the surface, increasing their residence times close to the wall and eventually leading to adhesion [28,29]. However, highly curved convex walls can remove this trapping effect and direct bacterial motion away from the wall [30,31]. For instance, a critical radius was determined for cylindrical pillars, below which bacteria significantly reduce their residence time around the pillars [32]. The same principle has been used to direct and concentrate swimming bacteria [33].

Sinusoidal surfaces are a model geometrical pattern to study the possibilities of topography to control bacterial accumulation. In the valleys of a sinusoidally shaped surface, the cells reorient themselves and are guided toward the peaks. There, they detach from the wall due to its curvature. It has been proven that accumulation of *Escherichia coli* on this kind

*Corresponding author: benjamin.perez-estay@espci.fr

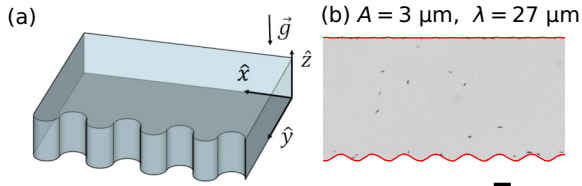


FIG. 1. (a) Diagram of a section of the microfluidic device with constant amplitude and wavelength. (b) Snapshot obtained in a device with $A = 3 \mu\text{m}$ and $\lambda = 27 \mu\text{m}$. Color has been inverted, hence bacteria appear dark. The red lines represent the vertical walls of the channel and the scale bar is $10 \mu\text{m}$.

of surface can reduce up to 50 % when compared to a flat surface thanks to this phenomenon [34]. Additionally, the authors suggest curvature at the valley as a parameter to characterize the optimal topography for reducing accumulation. However, we still lack an understanding of why valley curvature defines the optimal boundary and to what extent it determines the accumulation. In this paper, we characterize the dynamics of the bacteria interacting with a sinusoidal surface to answer these questions. Interestingly, we find three different accumulation regimes and show that the principal observables depend mainly on the characteristic curvature of the surface, showing a nonmonotonic behavior. Also, in contrast to the aforementioned work, we studied both smooth swimming and tumbling bacteria, finding that tumbling only marginally affects the results. Simulations of a minimal model show that the bacterial accumulation can be both quantitatively and qualitatively well described considering only the steric interactions with the surface. Using these results, we present theoretical arguments to show that beyond a critical curvature, which matches experimental results, swimming along the walls becomes unstable and instead the perpendicular orientation is favored.

II. EXPERIMENTAL SETUP

We use two strains of fluorescent *E. coli* bacteria: JEK1036, which performs usual run and tumbles (R&T), and JEK1038, which is mutated to suppress tumble (smooth swimmers, SS). Each strain is used separately, suspended in motility buffer in dilute conditions (optical density at 600 nm $\text{OD}_{600} = 5 \times 10^{-4}$, corresponding to, approximately, 5×10^5 bact/mL). The suspensions are injected into long, $100 \mu\text{m}$ -wide and $25 \mu\text{m}$ -deep PDMS microfluidic channels, fabricated with standard soft lithography techniques [35]. The microfluidic devices have three flat walls and a fourth undulated one in a sinusoidal form, $A \sin(2\pi x/\lambda)$. Each microchannel has sections of length 1 mm with multiple sinusoidal periods of constant amplitude A and wavelength λ , as shown in Fig. 1(a). We work with 16 combinations of parameters (A , λ), with nominal values $A = 3, 6, 9, 12 \mu\text{m}$ and $\lambda = 21, 24, 27, 30 \mu\text{m}$. The actual amplitude and wavelength of the sinusoidal walls can differ up to 17 % from the nominal values due to imperfections of the microfabrication procedure. For each case, we measure the real amplitude and wavelength using fluorescence microscopy.

Prior to the injection, the channels are filled with 0.1% BSA solution dissolved in motility buffer to prevent cell

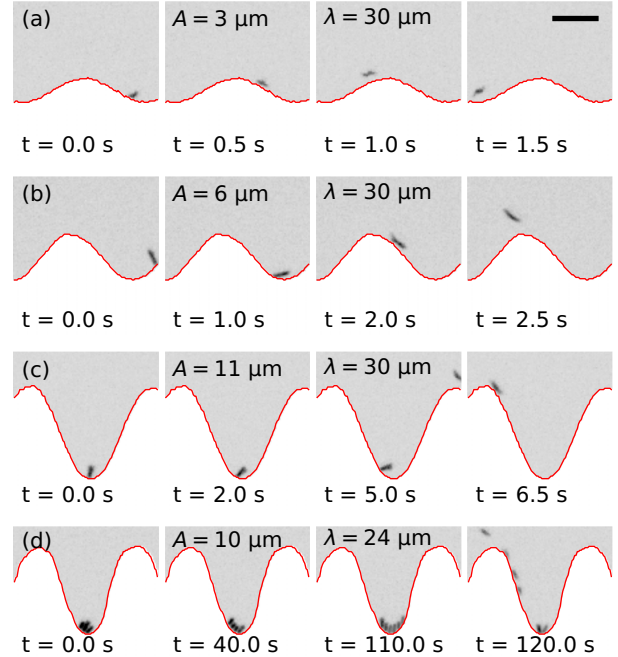


FIG. 2. Color-inverted snapshot sequences obtained with fluorescence microscopy, showing smooth swimmers as they move in contact with curved walls of different amplitudes A and wavelengths λ , with increasing curvature from top to bottom. Times indicated at the bottom of each frame are with respect to the first contact of the bacterium with the wall, except for (d), in which the cluster existed already at the beginning of the acquisition. The red lines mark the measured position of the walls. The scale bar in the top right represents $10 \mu\text{m}$. Corresponding movies S1, S2a, S3a, and S4 are available in the Supplemental Material [37].

adhesion to walls. After inoculation, the inlets of the channel are sealed with glass coverslips to prevent residual flow. We image the bacteria in fluorescence using an inverted microscope (Nikon TS100F) with a $40\times/0.6 \text{ NA}$ Plan Fluor objective. Videos are recorded for 2 min at 10 fps with a digital camera (Andor Zyla 4.2). The focal plane is located at the bottom of the channel ($z = 0$). Figure 1(b) shows a typical frame obtained in the experiments. Bacteria are tracked in two dimensions using the TrackMate plug-in of Fiji [36].

III. EXPERIMENTAL RESULTS

A. Global and local accumulation of bacteria at the curved walls

To study the interaction and accumulation of bacteria at curved surfaces, we proceed to perform experiments at low concentration, allowing us to follow the motion of individual swimmers. When swimming near a wall with low curvature, SSs can follow the sinusoidal surface due to hydrodynamic effect [9,27,32] and steric alignment, much like near a flat wall. An example is shown in Fig. 2(a) and Supplemental Material video S1 [37]. As curvature increases, this hydrodynamic effect is not strong enough, making it more likely that bacteria leave the surface once they reach a peak of the sinusoidal wall. This kind of trajectory can be observed in Fig. 2(b) and the corresponding Supplemental Material video

S2a [37]. Another example is shown in Supplemental Material video S2b [37].

For walls with even higher curvature, alignment is insufficient to rotate the swimmers when they reach a valley, resulting in bacteria swimming nearly perpendicular to the surface. This effect causes bacteria to stay in the valleys for several seconds before, eventually escaping thanks to fluctuations, as can be seen in Fig. 2(c) and the corresponding Supplemental Material video S3a [37]. Note that this happens independently of the angle with which the bacterium impacts the wall. For illustration, another two examples with bacteria coming from the right and left of the valley are available in the Supplemental Material videos S3b and S3c [37]. In both cases, the bacteria swim along the walls until becoming trapped at the valley.

The time that bacteria remain trapped in the valleys increases dramatically as curvature increases further, which could lead to the arrival of multiple bacteria at the same valley. Bacteria-bacteria interactions suppress the alignment with the surface, and clusters of bacteria can remain for several minutes. Clusters formed in this manner exhibit a stable aligned state. An example is shown in Fig. 2(d) and Supplemental Material video S4 [37]. The dispersion of the cluster normally follows the destabilization caused by swimming noise or the arrival of new bacteria.

Based on these observations, we measure bacterial accumulation at the curved walls. For this, we select the bacteria that are in contact with either the curved or flat surface, where the contact bands are defined as a region $4\ \mu\text{m}$ from each surface in the $\pm y$ direction for the flat and curved wall, respectively [see Fig. 1(a) for the definition of the coordinate system]. From the tracking of this subset, the bacterial density along the curved and flat surfaces, respectively, $\mu'_{\text{curved}}(x)$ and $\mu'_{\text{flat}}(x)$, are obtained by averaging over time. To reduce the statistical error, we average μ'_{curved} over the different oscillation periods and collapse it on the interval $-\lambda/2$ to $\lambda/2$, centered around the valley. Also, as the global bacterial concentration varies between experimental realizations, for each experiment we normalize the mean bacterial density on the curved surface to the spatial average of the flat one: $\mu(x) = \mu'_{\text{curved}}(x) / \langle \mu'_{\text{flat}}(x) \rangle_x$. Therefore, values of $\mu(x)$ larger than unity indicate an accumulation of bacteria at the curved wall in comparison with the flat one.

Figure 3(a) presents the normalized density profiles $\mu(x)$ for the cases shown in Figs. 2(a)–2(c), which have equal wavelength but increasing amplitudes. For amplitudes $A = 3, 6\ \mu\text{m}$, the bacterial density is roughly flat, with an average value smaller than unity that decreases with the amplitude, meaning that bacteria accumulate less in the curved wall with $A = 6\ \mu\text{m}$ than in the one with $A = 3\ \mu\text{m}$. This can be understood by the ejection of bacteria at the peaks from the most curved wall, as shown in Fig. 2(b). Conversely, for $A = 9, 11\ \mu\text{m}$, a maximum at $x = 0$ appears which increases with the amplitude, consistent with the bacteria accumulation at the valley observed in this case [Fig. 2(c)].

There is an asymmetry on the profiles with respect to the center of the valleys at $x = 0$ for $A = 3\ \mu\text{m}$ and some cases with $A = 6\ \mu\text{m}$, with more bacteria on the left half of the period. This asymmetry is caused by the counterclockwise circular motion of bacteria when swimming near the bottom

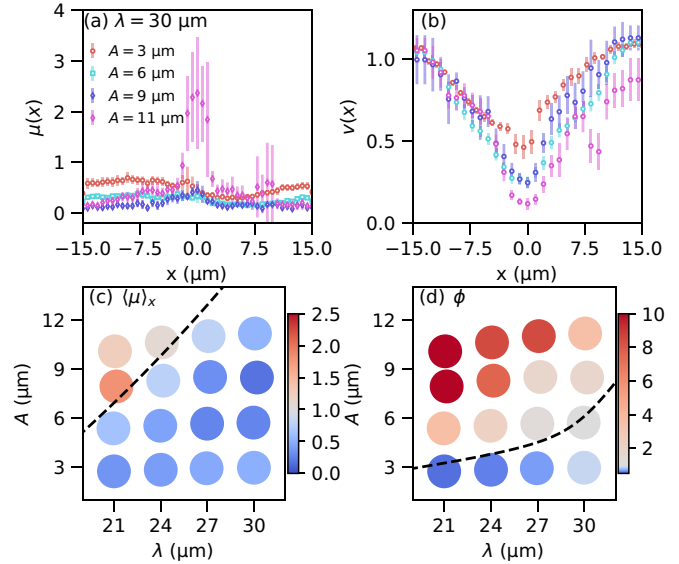


FIG. 3. Normalized linear density (a) and normalized average speed of swimmers in contact with the curved walls (b) as a function of x for three cases with constant wavelength $\lambda = 30\ \mu\text{m}$ and varying amplitude A . Error bars represent the 95 % confidence interval for the mean. (c) Spatial average of the normalized concentration profile as a function of the measured amplitudes and wavelengths, A and λ . The number of surface periods considered in the averages is indicated above each data point. (d) Valley to peak density ratio, ϕ , as a function of the measured amplitudes and wavelengths, A and λ . The dashed black curves show $\langle \mu \rangle_x = 1$ and $\phi = 1$, obtained from fitting the measurements to a second order polynomial in A and λ . For ϕ , the fit is performed only with data points near the region of interest.

surface [27]. When bacteria swim from right to left and leave the surface on the peak at the left of the valley, the trajectory will curve toward the surface, thanks to the counterclockwise circular trajectory, naturally increasing the density on the left side of the profile. On the contrary, bacteria leaving on the peak at the right of the valley will be directed away from the surface (see Fig. 4 and corresponding Supplemental Material

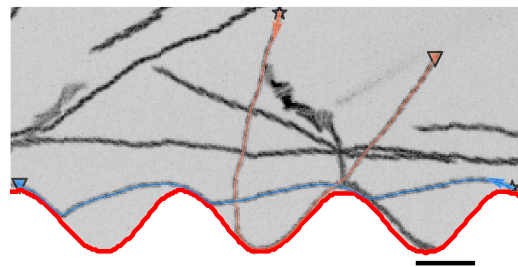


FIG. 4. Examples of bacteria trajectories. The initial and final positions are represented by a star and a triangle, respectively. Due to the counterclockwise rotation at the surface, the orange trajectory leaves the curved surface at the right of the valley, so it curves out, while the opposite happens several times to the blue trajectory. The red lines represent the measured walls of the channel, and the scale bar is $10\ \mu\text{m}$. The background is a superposition of color-inverted frames in a time interval of 5 s. The corresponding movie S5 is available in the Supplemental Material [37].

video S5 [37]). Additionally, one could think that this chiral effect biases the detachment from the peaks. Nevertheless, even for the lowest curvature of $0.13 \mu\text{m}^{-1}$, bacteria briefly detach from the surface for any side of the peak. Therefore, circular trajectories due to interactions with the bottom flat surface play an important role only away from the lateral flat and sinusoidal walls, causing bacteria to swim apart from the wall systematically, or toward it, depending on the swimming direction.

The average velocity on the curved side as a function of the position on the period was also measured from the tracking of bacteria in the contact bands. To reduce the deviations produced by the variability in bacterial activity from experiment to experiment, the average velocities were normalized by the average speed of bacteria in the bulk for each experiment (typically about $20 \mu\text{m s}^{-1}$). Figure 3(b) shows the normalized velocity profiles, $v(x)$, for the same cases of Fig. 3(a). Consistent with the observed behavior, the velocity is smaller near the valley, with decreasing values as the amplitude increases.

The global relative accumulation of bacteria at the curved wall was defined as the spatial average of the normalized density profiles, $\langle \mu \rangle_x$. Figure 3(c) shows $\langle \mu \rangle_x$ as a function of A and λ . Values smaller than one, which happen for most of the cases, mean that less global accumulation on the curved surface occurs compared to the flat one. The transition curve $\langle \mu \rangle_x = 1$ was determined from a quadratic fit to the experimental data, and is shown as the dashed line in Fig. 3(c). The transition occurs for amplitudes $A > 6 \mu\text{m}$ in the range of wavelengths considered, and is outside of the experimental set for $\lambda > 27 \mu\text{m}$. Indeed, in most of the studied parameter space, $\langle \mu \rangle_x$ is smaller than one. There is a minimum at $A = 9 \mu\text{m}$ and $\lambda = 30 \mu\text{m}$, with $\langle \mu \rangle_x = 0.2$, considerably smaller than one. Cases with evident accumulation at the valleys, such as the example of Fig. 2(c), still yield an average global bacterial density $\langle \mu \rangle_x < 1$, which shows that this metric does not reflect completely the onset of accumulation in the curved walls.

The preferential bacterial accumulation at the valleys is characterized by the probability of finding bacteria there. For that, we define ϕ as the ratio of integrated bacterial density on the valleys to the integral outside the valley:

$$\phi = \frac{\int_{-\lambda/4}^{\lambda/4} \mu(x) dx}{\int_{-\lambda/2}^{-\lambda/4} \mu(x) dx + \int_{\lambda/4}^{\lambda/2} \mu(x) dx}. \quad (1)$$

Figure 3(d) presents ϕ as a function of A and λ . The dashed curve represents $\phi = 1$, obtained by a quadratic fit of the data, separating the regions where there is an excess of bacteria in the valleys ($\phi > 1$) to those where is a deficit ($\phi < 1$).

Comparing Figs. 3(c) and 3(d), three regions are clearly identified. For large curvatures (small wavelength and large amplitudes), $\langle \mu \rangle_x > 1$ and $\phi > 1$, meaning that, on average, more bacteria accumulate on the undulated wall, with preference for the valleys. In the opposite limit of small curvatures (large wavelengths and small amplitudes), $\langle \mu \rangle_x < 1$ and $\phi < 1$, implying that, on average, the undulated wall captures less bacteria than the flat one and they preferentially accumulate at the peaks. In the intermediate region, the average accumulation on the undulated wall is smaller than on the flat one but,

nevertheless, at the valleys there is an increasing concentration of bacteria.

B. Effect of curvature

The two effects that explain the different behaviors of bacteria swimming near the walls, i.e., bacteria alignment to the wall and bacteria trapping at the valleys, depend on the curvature of the wall. Starting from a flat concentration profile for a flat wall, the accumulation of bacteria at the walls decreases with increasing curvatures as bacteria leave more easily the surfaces at the peaks. For larger curvatures, bacteria get trapped in the valleys, increasing the accumulation for the higher curvatures. This nonmonotonic dependence suggests that a minimum of accumulation should occur for a critical value of curvature.

Since the valleys and the peaks are key to determining the dynamics of bacteria, it is natural to study the system with respect to the curvature of the wall in those positions, given by $\kappa = 4\pi^2 A/\lambda^2$. Figures 5(a) and 5(b) show the average normalized density $\langle \mu \rangle_x$ and the valley to peak density ratio ϕ as functions of κ . The collapse of data shows that bacterial accumulation on curved surfaces is primarily determined by the maximum curvature of the wall. In the limit of vanishing curvature, the flat surface is recovered, implying that there one should get $\langle \mu \rangle_x = 1$ and $\phi = 1$, which are shown with a star in the figures. The average density presents the nonmonotonic behavior described before, with a minimum accumulation for $\kappa_{\text{min}} \approx 0.4 \mu\text{m}^{-1}$, in agreement with the previously published result of $0.31 \mu\text{m}^{-1}$ [34]. Only for curvatures larger than $0.7 \mu\text{m}^{-1}$, the average accumulation on the curved wall becomes larger than the flat one.

The ratio ϕ equals one at a critical curvature. Values smaller than one are measured for small curvatures, meaning that in those cases the maximum accumulation, although weak, occurs at the peaks. Conversely, ϕ is greater than one and with large values for large curvatures, corresponding to preferential accumulation at the valleys. The transition takes place for $\kappa^* \approx 0.25 \mu\text{m}^{-1}$.

The residence time of bacteria in the contact zones of the curved surfaces was also measured from bacterial tracking. Leaving contact was defined as being away from the contact zones for longer than 0.5 s, that is, not returning to the surface before that time. The average contact times τ are shown in Fig. 5(c). Although there is a large dispersion, the average residence time remains constant around 1.5 s for curvatures smaller than the critical value κ^* . We could not measure the residence times in the flat wall because they are too long for our experimental setup: Frequently, bacteria enter or leave the field of view while in contact with the flat wall, hence biasing the measured times to shorter values. However, when compared to what has been reported for flat surfaces [28], contact times for curvatures smaller than κ^* are one order of magnitude smaller. For larger curvatures, the average of τ increases as bacteria start to be trapped in the valleys. The residence times show large dispersion, with some bacteria reaching the curved wall near a peak and leaving it shortly after, while some other remaining very long in a valley. For curvatures larger than $0.7 \mu\text{m}^{-1}$, bacteria start to form clusters more often and tracking of individual bacteria for long times

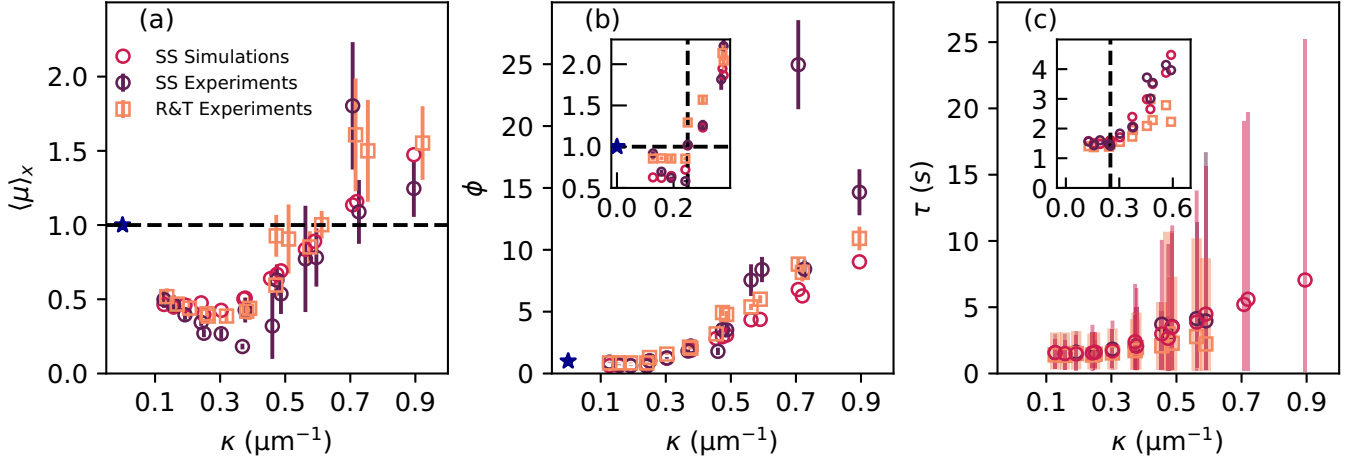


FIG. 5. (a) Average accumulation at the curved wall $\langle \mu \rangle_x$, (b) valley to peak density ratio ϕ , and (c) residence time τ as a function of the maximum curvature of the walls, $\kappa = 4\pi^2 A/\lambda^2$. As a reference, the theoretical values for vanishing curvature $\langle \mu \rangle_x = 1$, $\phi = 1$ are shown with a star in (a) and (b). For $\langle \mu \rangle_x$ and ϕ , error bars represent the 95% confidence interval for the average of the parameter. For the contact times, they represent the interval that contains 90% of the measured contact times. Contact times for curvatures $\kappa > 0.7 \mu\text{m}^{-1}$ are immeasurable due to the formation of clusters. The insets show a zoom of the small curvature region where the dashed lines are reference values of $\mu = 1$, $\phi = 1$, and $\kappa = \kappa^* = 0.25 \mu\text{m}^{-1}$.

becomes more difficult. Therefore, residence times are not reported in those cases.

C. Run-and-tumble swimmers

The behavior of R&T swimmers is qualitatively similar to SS and, quantitatively, only slight changes are observed. Figure 5 includes the mean normalized bacterial density $\langle \mu \rangle_x$, the valley to peak density ratio ϕ , and the contact times τ as a function of the maximum wall curvature κ for R&T. The average normalized density $\langle \mu \rangle_x$ for R&T swimmers [Fig. 5(a)] retains its nonmonotonic dependence with the curvature. In comparison with SS, $\langle \mu \rangle_x$ for R&T swimmers is larger, because tumbles facilitate escaping from the flat wall, therefore affecting the normalization. Although this effect also helps bacteria escaping from the curved wall, ejection at the peaks is dominant in this case and tumbling does not appreciably change the bacterial density at the curved wall. The minimum accumulation takes place at a similar curvature $\kappa_{\min} \approx 0.3 \mu\text{m}^{-1}$ than for the SS.

The value of ϕ for R&T [Fig. 5(b)] is also smaller than one for low curvatures and becomes larger than one at the same κ^* . In comparison with SS, the values of ϕ for R&T before the transition are larger. This is because, while the ejection of bacteria at the peaks, together with the swimming persistence, prevented SS to reach the valleys, in this case R&T can approach the walls in any position, thus making ϕ closer to 1.

The residence time [Fig. 5(c)] behaves similarly as for SS, with large dispersion but a relatively constant average value at around 1.5 s for low curvatures and starting to increase when bacteria begin to be trapped. Nevertheless, the average values are smaller because tumbling facilitates bacteria escaping from the walls. In any case, the effects of the valley to trap bacteria are clear when looking at $\langle \mu \rangle_x$ and τ , revealing that the tumbling of bacteria does not alter either the capacity of

the surface to remove bacteria at low curvature or the critical curvature for the onset of accumulation at the valleys.

IV. SIMULATIONS

To capture the essential dynamics of the system, we simulate active Brownian particles (ABP) moving in two dimensions [38], with periodic boundary conditions on the lateral directions and confined by a flat and a sinusoidal wall. By doing so, we eliminate the possibility for bacteria to approach from and escape to the third dimension. In the simulations, we neglect the circular motion of the swimmers in contact with the bottom and upper walls [27], which although gives rise to the small asymmetry on the density profiles, is subdominant for the reported phenomena, as well as translational noise, which is negligible compared to self-propulsion.

Each swimmer is described by its position \mathbf{r} and director $\hat{\mathbf{p}} = (\cos \theta, \sin \theta)$, where the director angle θ is subject to rotational noise of intensity D_r . The swimmers are modeled as disks with radius L_{cm} . We focus on the dilute regime, so particle interactions, both hydrodynamic and steric, are negligible. Swimmers do, however, interact with the walls. The total force on each swimmer, which vanishes in the low-Reynolds regime, is $\gamma u \hat{\mathbf{p}} + F_{\text{wall}} \hat{\mathbf{n}}_{\text{wall}}$, where γ is the viscous drag coefficient, u is the self-propulsion speed of the swimmers, and $\hat{\mathbf{n}}_{\text{wall}}$ the local unit vector normal to the wall, pointing into the swimming domain. The force exerted by the wall when swimmers are in contact with it is obtained by imposing $\dot{\mathbf{r}} \cdot \hat{\mathbf{n}}_{\text{wall}} = 0$, resulting in $F_{\text{wall}} = -\gamma u \hat{\mathbf{p}} \cdot \hat{\mathbf{n}}_{\text{wall}}$.

When bacteria are in contact with a wall, hydrodynamic and steric interactions induce an alignment of the swimmer to the surface [26,32]. In simulations, this effect is modeled as a torque, τ_{wall} , associated with the force from the wall, which we assumed is applied in the bacterium at a position $L_{\text{cm}} \hat{\mathbf{p}}$ with respect to the swimmer center of mass. This gives $\tau_{\text{wall}} = (L_{\text{cm}} \hat{\mathbf{p}} \times F_{\text{wall}} \hat{\mathbf{n}}_{\text{wall}}) \cdot \hat{\mathbf{z}} = -u L_{\text{cm}} \gamma (\hat{\mathbf{p}} \cdot$

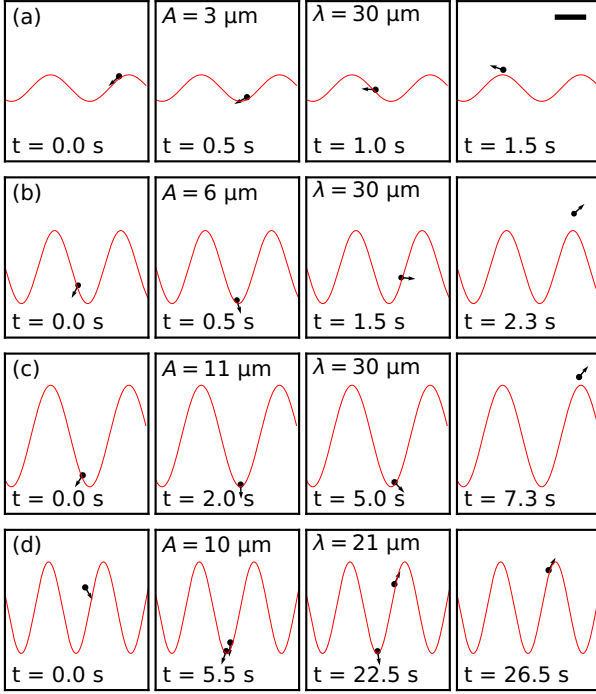


FIG. 6. Simulation snapshots, analog to Fig. 2, showing smooth swimmers moving in contact with the surface. Times indicated at the bottom of each frame are with respect to the first contact of the particle with the wall. The red lines mark the position of the walls and the scale bar is equivalent to $10\ \mu\text{m}$. Corresponding movies S6–S9 are available in the Supplemental Material [37].

$\hat{\mathbf{n}}_{\text{wall}})(\hat{\mathbf{p}} \cdot \hat{\mathbf{t}}_{\text{wall}})$, where $\hat{\mathbf{t}}_{\text{wall}} = \hat{\mathbf{n}}_{\text{wall}} \times \hat{\mathbf{z}}$ is the tangent to the wall.

In summary, the equations of motion for each SS are

$$\dot{\mathbf{r}} = u\hat{\mathbf{p}} - u(\hat{\mathbf{p}} \cdot \hat{\mathbf{n}}_{\text{wall}})\hat{\mathbf{n}}_{\text{wall}}\Gamma(\mathbf{r}, \hat{\mathbf{p}}), \quad (2)$$

$$\dot{\theta} = -(\hat{\mathbf{p}} \cdot \hat{\mathbf{n}}_{\text{wall}})(\hat{\mathbf{p}} \cdot \hat{\mathbf{t}}_{\text{wall}})\Gamma(\mathbf{r}, \hat{\mathbf{p}})/T + \sqrt{2D_r}\eta(t), \quad (3)$$

where $T = (uL_{\text{cm}}\gamma/\gamma_r)^{-1}$ is the steric reorientation time, with γ_r the rotational drag coefficient, η is a white noise, and $\Gamma(\mathbf{r}, \hat{\mathbf{p}})$ is a Heaviside step function, equal to one if the particle is in contact with the surface and swimming towards it. The equations are integrated with the forward Euler scheme.

Based on the experimental results, we use $u = 20\ \mu\text{m s}^{-1}$ and $L_{\text{cm}} = 0.5\ \mu\text{m}$. Given that the bacteria of the experiment resemble elongated spherocylinders instead of perfect spheres, the two parameters D_r and T were fitted to better reproduce the experimental observable ϕ for SS in the simulations [Fig. 3(d)]. The optimal values thus found are $T = 0.26\ \text{s}$ and $D_r = 0.04\ \text{rad}^2\ \text{s}^{-1}$. With these values, the model adequately reproduces the average density $\langle \mu \rangle_x$, the valley to peak density ratio ϕ , and the average contact times τ , as shown in Fig. 5.

The model does not only reproduce the macroscopic properties but also the dynamics of individual swimmers. Figure 6 shows simulated swimmer trajectories for a wall with curvature $\kappa < \kappa_{\text{min}}$ [Fig. 6(a) and Supplemental Material video S6 [37]], $\kappa_{\text{min}} < \kappa < \kappa^*$ [Fig. 6(b) and Supplemental Material video S7 [37]], and $\kappa > \kappa^*$ [Figs. 6(c) and 6(d) and

Supplemental Material videos S8 and S9 [37]]. In the latter, the absence of swimmer-swimmer interactions prevents the formation of clusters of trapped swimmers.

In the case of including tumbling, a new director angle is chosen at random with a rate ν_{tumble} . Here, a third parameter is added to the model, which is fitted as for SS to best reproduce the experimental measurements of ϕ , obtaining $\nu_{\text{tumble}} = 1/7.0\ \text{s}$. The results of the simulation for the average accumulation, the valley to peak density ratio, and the residence times as a function of the curvature (not shown to avoid overcrowding the plots) are in very good agreement with the experiments and, as for the experiments, do not differ appreciably to the results for SS.

The successful comparison with the experiments shows that the observed phenomena we report are mainly due to the steric interactions of swimmers with the walls, in accordance with Ref. [34]. That is, we were able to reproduce qualitatively and quantitatively the observed phenomena without appealing to hydrodynamic attraction to the walls or to the velocity reduction due to lubrication effects.

V. CRITICAL CURVATURE

The simulations show that the accumulation of bacteria at curved surfaces can be well described by a simple model where the swimmers self-propel and interact sterically with the surface. This interaction is responsible for aligning bacteria to the surface. With this model in mind, we can compute the critical curvature as follows. Consider, for simplicity, that the curvature κ of the wall is fixed and that the swimmer with director $\hat{\mathbf{p}}$ is already interacting with the surface, with $\hat{\mathbf{t}}_{\text{wall}}$ and $\hat{\mathbf{n}}_{\text{wall}}$ the local tangential and normal unit vectors to the surface. To characterize the orientation of the swimmer with respect to the surface, we define $\xi = \hat{\mathbf{p}} \cdot \hat{\mathbf{t}}_{\text{wall}}$, such that $\xi = \pm 1$ means complete alignment with the surface and $\xi = 0$ is when it is perpendicular to the surface. Considering that the normal points into the swimming domain, that gives $\hat{\mathbf{p}} \cdot \hat{\mathbf{n}}_{\text{wall}} = -\sqrt{1 - \xi^2}$.

To compute the time derivative, $\dot{\xi} = \dot{\hat{\mathbf{p}}} \cdot \hat{\mathbf{t}}_{\text{wall}} + \hat{\mathbf{p}} \cdot \dot{\hat{\mathbf{t}}_{\text{wall}}}$, the noiseless version of Eq. (3) for a swimmer in contact with the surface dictates that $\dot{\hat{\mathbf{p}}} = \dot{\theta} \hat{\mathbf{z}} \times \hat{\mathbf{p}}$, with $\dot{\theta} = -(\hat{\mathbf{p}} \cdot \hat{\mathbf{t}}_{\text{wall}})(\hat{\mathbf{p}} \cdot \hat{\mathbf{n}}_{\text{wall}})/T$. The temporal derivative of the tangential vector is obtained from the kinematics on a curved trajectory,

$$\dot{\hat{\mathbf{t}}_{\text{wall}}} = \frac{d\hat{\mathbf{t}}_{\text{wall}}}{ds} \frac{ds}{dt}, \quad (4)$$

where s is the arc length. Differential geometry gives $d\hat{\mathbf{t}}_{\text{wall}}/ds = \kappa \hat{\mathbf{n}}_{\text{wall}}$, where, according to our election of signs for the unit vectors, κ is positive in the valleys. Finally, the tangential velocity is simply the projection of \mathbf{u} along the trajectory, $\frac{ds}{dt} = u\hat{\mathbf{p}} \cdot \hat{\mathbf{t}}_{\text{wall}}$. Collecting all terms, and using that $(\hat{\mathbf{z}} \times \hat{\mathbf{p}}) \times \hat{\mathbf{t}}_{\text{wall}} = -\hat{\mathbf{p}} \cdot \hat{\mathbf{n}}_{\text{wall}}$, gives

$$\dot{\xi} = \xi \sqrt{1 - \xi^2} (\sqrt{1 - \xi^2} - \kappa T) / T. \quad (5)$$

This equation shows that ξ presents five fixed points. Of these, $\xi = \pm 1$ are unstable for any positive curvature and can be neglected for the analysis. For $\kappa T < 1$, $\xi = 0$ is unstable and $\xi = \pm \sqrt{1 - (\kappa T)^2}$ are stable fixed points, corresponding to configurations where the swimmers move along the

surfaces, forming an angle with respect to the surface $\theta = \sin^{-1}(u\kappa T)$ either to the right or left. The swimming angle increases with the curvature until $u\kappa T = 1$, where it becomes perpendicular. For larger curvatures, now the perpendicular configuration (fixed point $\xi = 0$) becomes stable and the other fixed points disappear. The transition takes place when the aligning torque, represented by the first term in Eq. (5), is not able to compensate the continuous change in the direction of the tangent vector, which is accounted for by the second term in the equation. The change of stable configurations when varying the curvature is indeed observed in our experiments. Movies S3b and S3c in the Supplemental Material [37] first show the bacterial alignment when they reach the walls at a low curvature region. This is followed by the bacteria motion sliding along the wall toward the valley and can be clearly noticed at a point where now bacteria becomes perpendicular to the wall as an effect of the larger curvature in this region.

Hence, we have identified a critical curvature of $\kappa_{\text{theo}}^* = 1/(uT) = L_{\text{cm}}\gamma/\gamma_r$, such that surfaces with higher curvatures will trap the bacteria, making them swim perpendicular to the surface. The drag coefficients scale as $\gamma \sim L_{\text{cm}}$ and $\gamma_r \sim L_{\text{cm}}^3$, with prefactors that depend on the geometry of the swimmer, implying that $\kappa_{\text{theo}}^* \sim L_{\text{cm}}^{-1}$. The critical curvature is hence controlled by the bacterial length and its geometry. The parameters used in the simulation give $\kappa_{\text{theo}}^* = 0.2 \mu\text{m}^{-1}$, which is comparable to the value of $\kappa^* = 0.25 \mu\text{m}^{-1}$ obtained from the experiments.

One key aspect of the derivation is that we assumed fixed positive curvature. Therefore, swimmers moving inside circular surfaces would remain trapped if the curvature is larger than the critical. Nevertheless, in simulations and experiments with a sinusoidal wall, the curvature decreases when bacteria swim away from the valley. This, coupled with the presence of rotational diffusion leads to the possibility of exiting the trap even for curvatures larger than the critical. The balance between curvature and rotational diffusion defines the time bacteria are trapped in the valley of sinusoidal surfaces.

VI. DISCUSSION AND CONCLUSIONS

Using experiments of nontumbling and R&T strains of *E. coli* swimming in microfluidic devices with fabricated sinusoidal walls of controlled amplitudes and wavelengths, we have studied the interaction of these bacteria with curved walls and the accumulation that results. This geometry was previously considered in Ref. [34] where, doing experiments using a nontumbling strain of *E. coli* and simulations of tumbling and nontumbling models of swimmers, it was found that bacteria accumulate preferentially in the valleys of the undulated wall and identified a critical curvature for minimal accumulation. Here we define appropriate metrics to characterize the global accumulation on the curved wall compared to the reference flat one on the opposite side of the channel, as well as the spatial distribution of swimmers on the the curved wall. For both strains of bacteria, those metrics show that the accumulation process is controlled mainly by the maximum curvature κ of the curved wall and not separately by the amplitude or wavelength. The dependence on the curvature is not monotonic and three regimes are identified. For low curvatures, $\kappa < 0.25 \mu\text{m}^{-1}$, the curved wall captures less bacteria than the

flat one and the bacteria that are close to the curved wall show a weak preference to be located close to the sinusoidal peaks. For curvatures in the range $0.25 \mu\text{m}^{-1} < \kappa < 0.7 \mu\text{m}^{-1}$, the average accumulation on the curved wall is still smaller than on the flat wall, but now bacteria are preferentially located at the valleys. Finally, for curvatures larger than $0.7 \mu\text{m}^{-1}$, the average accumulation on the curved wall is larger than on the flat one and the number of bacteria in the valleys starts to grow rapidly with curvature, forming long-lived clusters.

The three regimes can be qualitatively well understood by following the kinematics of bacteria swimming near the walls, where we were able to identify that, for low curvatures, bacteria can persistently swim parallel to the walls. When increasing the curvature, bacteria align with the surface and are ejected near the peaks. For curvatures below $0.4 \mu\text{m}^{-1}$, the contact times with the surface are smaller than 2 s on average, and they start to grow considerably for larger curvatures. Finally, when the curvature is too large, alignment is not possible and bacteria are trapped on the valleys, which can even lead to the formation of clusters. When clusters are formed, tracking becomes difficult and it is not possible to obtain the contact times accurately, but values larger than 200 s were observed. These increasing contact times make it more likely for bacteria to adhere to the surface.

Although hydrodynamic interactions between the walls and the bacteria are undoubtedly present, as evidenced by the decrease of bacteria speed near the walls, we demonstrated numerically that they are not relevant to describe the bacterial accumulation. A minimal computational model was simulated, where we consider active Brownian particles moving on two dimensions, interacting only sterically with the walls, which reorient the swimmers as a result of being impenetrable. Fitting the rotational Brownian diffusivity and the reorientation time, the model accurately captures the observed phenomena. This result allowed us to build a dynamical model with which the critical curvature that controls the accumulation on the valleys is accurately predicted and is shown to be inversely proportional to the bacterial body length. The success of the simulations and the dynamical model confirms that the reorientation and escape dynamics are controlled mainly by curvature and the steric bacterial-wall interactions. The clustering that follows, but not the accumulation, depends strongly on mutual bacterial interactions and, consequently, our model fails to predict them, as can be seen in the different observables at high curvature.

In our experiments, we do not allow for bacteria to divide and, also, the treatment of the surfaces impedes bacteria to adhere. Consequently, no biofilm is form, even in cases where crowding was observed in the valleys. Nevertheless, our results give important information on the early stages of bacterial accumulation: The recognition of three different regimes and the nonmonotonic dependence with curvature should be considered in designing devices aiming to control bacterial accumulation. For example, the sole quantification by the average accumulation can produce misleading results as it is possible to have less bacteria on average on the curved wall, but the formation of clusters in the valleys. Since clustering of bacteria can potentially lead to infection foci, this is key to design curved surfaces that avoid bacterial accumulation.

ACKNOWLEDGMENTS

This research was supported by the ANID, Millennium Science Initiative Program No. NCN19_170 and ANID, Fondecyt Grants No. 1220536 (R.S. and N.S.) and No. 1210634 (M.L.C.), all from ANID, Chile, and the Franco–Chilean Ecos–Sud Collaborative Program No. ECOS210012/ECOS_C21E05. Fabrication of microfluidic

devices was possible thanks to ANID Fondecyt Grants No. EQM140055 and No. EQM180009. This project received funding from the European Union’s Horizon 2020 research and innovation program under the Marie Skłodowska-Curie Grant Agreement No 955910. We also thank E. Clement and A. Lindner for fruitful discussions, and J. Rodríguez for preliminary experiments.

-
- [1] C. R. Arciola, D. Campoccia, and L. Montanaro, Implant infections: Adhesion, biofilm formation and immune evasion, *Nat. Rev. Microbiol.* **16**, 397 (2018).
- [2] J. Costerton, L. Montanaro, and C. R. Arciola, Biofilm in implant infections: Its production and regulation, *Int. J. Artif. Organs* **28**, 1062 (2005).
- [3] S. Veerachamy, T. Yarlagadda, G. Manivasagam, and P. K. Yarlagadda, Bacterial adherence and biofilm formation on medical implants: A review, *Proc. Inst. Mech. Eng., H* **228**, 1083 (2014).
- [4] M. Quirynen, M. De Soete, and D. Van Steenberghe, Infectious risks for oral implants: A review of the literature, *Clin. Oral Implants Res.* **13**, 1 (2002).
- [5] R. M. Donlan, Biofilm formation: A clinically relevant microbiological process, *Clin. Infect. Dis.* **33**, 1387 (2001).
- [6] W. G. Characklis, Bioengineering report: Fouling biofilm development: A process analysis, *Biotechnol. Bioeng.* **23**, 1923 (1981).
- [7] T. Mattila-Sandholm and G. Wirtanen, Biofilm formation in the industry: A review, *Food Rev. International* **8**, 573 (1992).
- [8] C. D. Rummel, A. Jahnke, E. Gorokhova, D. Kühnel, and M. Schmitt-Jansen, Impacts of biofilm formation on the fate and potential effects of microplastic in the aquatic environment, *Environ. Sci. Technol. Lett.* **4**, 258 (2017).
- [9] A. P. Berke, L. Turner, H. C. Berg, and E. Lauga, Hydrodynamic attraction of swimming microorganisms by surfaces, *Phys. Rev. Lett.* **101**, 038102 (2008).
- [10] H. H. Tuson and D. B. Weibel, Bacteria–surface interactions, *Soft Matter* **9**, 4368 (2013).
- [11] A. Jacobs, F. Lafolie, J. Herry, and M. Debroux, Kinetic adhesion of bacterial cells to sand: Cell surface properties and adhesion rate, *Colloids Surf., B* **59**, 35 (2007).
- [12] K. Marshall, R. Stout, and R. Mitchell, Selective sorption of bacteria from seawater, *Can. J. Microbiol.* **17**, 1413 (1971).
- [13] L. Hall-Stoodley, J. W. Costerton, and P. Stoodley, Bacterial biofilms: From the natural environment to infectious diseases, *Nat. Rev. Microbiol.* **2**, 95 (2004).
- [14] J. W. Costerton, K. J. Cheng, G. G. Geesey, T. I. Ladd, J. C. Nickel, M. Dasgupta, and T. J. Marrie, Bacterial biofilms in nature and disease., *Annu. Rev. Microbiol.* **41**, 435 (1987).
- [15] J. T. Rostøl and L. Marraffini, (Ph)ighting phages: How bacteria resist their parasites, *Cell Host Microbe* **25**, 184 (2019).
- [16] C. Matz and S. Kjelleberg, Off the hook—how bacteria survive protozoan grazing, *Trends Microbiol.* **13**, 302 (2005).
- [17] M. Chen, Q. Yu, and H. Sun, Novel strategies for the prevention and treatment of biofilm related infections, *Int. J. Mol. Sci.* **14**, 18488 (2013).
- [18] P. S. Stewart, Biophysics of biofilm infection, *Pathog. Dis.* **70**, 212 (2014).
- [19] D. Perera-Costa, J. M. Bruque, M. L. González-Martín, A. C. Gómez-García, and V. Vellido-Rodríguez, Studying the influence of surface topography on bacterial adhesion using spatially organized microtopographic surface patterns, *Langmuir* **30**, 4633 (2014).
- [20] S. T. Reddy, K. K. Chung, C. J. McDaniel, R. O. Darouiche, J. Landman, and A. B. Brennan, Micropatterned surfaces for reducing the risk of catheter-associated urinary tract infection: An *in vitro* study on the effect of Sharklet micropatterned surfaces to inhibit bacterial colonization and migration of uropathogenic *Escherichia coli*, *J. Endourol.* **25**, 1547 (2011).
- [21] K. Efimenko, J. Finlay, M. E. Callow, J. A. Callow, and J. Genzer, Development and testing of hierarchically wrinkled coatings for marine antifouling, *ACS Appl. Mater. Interfaces* **1**, 1031 (2009).
- [22] X.-Q. Dou, D. Zhang, C. Feng, and L. Jiang, Bioinspired hierarchical surface structures with tunable wettability for regulating bacteria adhesion, *ACS Nano* **9**, 10664 (2015).
- [23] Y. Yuan, M. P. Hays, P. R. Hardwidge, and J. Kim, Surface characteristics influencing bacterial adhesion to polymeric substrates, *RSC Adv.* **7**, 14254 (2017).
- [24] H.-W. Chien, X.-Y. Chen, W.-P. Tsai, and M. Lee, Inhibition of biofilm formation by rough shark skin-patterned surfaces, *Colloids Surf., B* **186**, 110738 (2020).
- [25] K. K. Chung, J. F. Schumacher, E. M. Sampson, R. A. Burne, P. J. Antonelli, and A. B. Brennan, Impact of engineered surface microtopography on biofilm formation of staphylococcus aureus, *Biointerphases* **2**, 89 (2007).
- [26] S. Bianchi, F. Saglimbeni, and R. Di Leonardo, Holographic imaging reveals the mechanism of wall entrapment in swimming bacteria, *Phys. Rev. X* **7**, 011010 (2017).
- [27] E. Lauga, W. R. DiLuzio, G. M. Whitesides, and H. A. Stone, Swimming in circles: Motion of bacteria near solid boundaries, *Biophys. J.* **90**, 400 (2006).
- [28] K. Drescher, J. Dunkel, L. H. Cisneros, S. Ganguly, and R. E. Goldstein, Fluid dynamics and noise in bacterial cell-cell and cell-surface scattering, *Proc. Nat. Acad. Sci. USA* **108**, 10940 (2011).
- [29] G. Junot, T. Darnige, A. Lindner, V. A. Martinez, J. Arlt, A. Dawson, W. C. K. Poon, H. Auradou, and E. Clément, Run-to-tumble variability controls the surface residence times of *E. coli* bacteria, *Phys. Rev. Lett.* **128**, 248101 (2022).
- [30] M. B. Wan, C. J. OlsonReichhardt, Z. Nussinov, and C. Reichhardt, Rectification of swimming bacteria and self-driven particle systems by arrays of asymmetric barriers, *Phys. Rev. Lett.* **101**, 018102 (2008).

- [31] C. O. Reichhardt and C. Reichhardt, Ratchet effects in active matter systems, *Annu. Rev. Condens. Matter Phys.* **8**, 51 (2017).
- [32] O. Sipos, K. Nagy, R. Di Leonardo, and P. Galajda, Hydrodynamic trapping of swimming bacteria by convex walls, *Phys. Rev. Lett.* **114**, 258104 (2015).
- [33] P. Galajda, J. Keymer, P. Chaikin, and R. Austin, A wall of funnels concentrates swimming bacteria, *J. Bacteriol.* **189**, 8704 (2007).
- [34] R. Mok, J. Dunkel, and V. Kantsler, Geometric control of bacterial surface accumulation, *Phys. Rev. E* **99**, 052607 (2019).
- [35] J. C. McDonald and G. M. Whitesides, Poly (dimethylsiloxane) as a material for fabricating microfluidic devices, *Acc. Chem. Res.* **35**, 491 (2002).
- [36] J. Y. Tinevez, N. Perry, J. Schindelin, G. M. Hoopes, G. D. Reynolds, E. Laplantine, S. Y. Bednarek, S. L. Shorte, and K. W. Eliceiri, TrackMate: An open and extensible platform for single-particle tracking, *Methods* **115**, 80 (2017).
- [37] See Supplemental Material at <http://link.aps.org/supplemental/10.1103/PhysRevE.109.054601> for video examples of experiments and simulations for various curvatures.
- [38] N. Sepúlveda and R. Soto, Universality of active wetting transitions, *Phys. Rev. E* **98**, 052141 (2018).